



3-D visualization of ensemble weather forecasts – Part 2: Warm conveyor belts

M. Rautenhaus et al.

This discussion paper is/has been under review for the journal Geoscientific Model Development (GMD). Please refer to the corresponding final paper in GMD if available.

3-D visualization of ensemble weather forecasts – Part 2: Forecasting warm conveyor belt situations for aircraft-based field campaigns

M. Rautenhaus¹, C. M. Grams², A. Schäfler³, and R. Westermann¹

¹Computer Graphics & Visualization Group, Technische Universität München, Garching, Germany

²Institute for Atmospheric and Climate Science, ETH Zürich, Zurich, Switzerland

³Deutsches Zentrum für Luft- und Raumfahrt, Institut für Physik der Atmosphäre, Oberpfaffenhofen, Germany

Received: 4 February 2015 – Accepted: 12 February 2015 – Published: 27 February 2015

Correspondence to: M. Rautenhaus (marc.rautenhaus@tum.de)

Published by Copernicus Publications on behalf of the European Geosciences Union.

Title Page

Abstract

Introduction

Conclusions

References

Tables

Figures



Back

Close

Full Screen / Esc

Printer-friendly Version

Interactive Discussion



Abstract

We present the application of interactive 3-D visualization of ensemble weather predic-
tions to forecasting warm conveyor belt situations during aircraft-based atmospheric re-
search campaigns. Motivated by forecast requirements of the T-NAWDEx-Falcon 2012
campaign, a method to predict 3-D probabilities of the spatial occurrence of warm
conveyor belts has been developed. Probabilities are derived from Lagrangian particle
trajectories computed on the forecast wind fields of the ECMWF ensemble prediction
system. Integration of the method into the 3-D ensemble visualization tool Met.3D,
introduced in the first part of this study, facilitates interactive visualization of WCB fea-
tures and derived probabilities in the context of the ECMWF ensemble forecast. We
investigate the sensitivity of the method with respect to trajectory seeding and forecast
wind field resolution. Furthermore, we propose a visual analysis method to quantita-
tively analyse the contribution of ensemble members to a probability region and, thus,
to assist the forecaster in interpreting the obtained probabilities. A case study, revisiting
a forecast case from T-NAWDEx-Falcon, illustrates the practical application of Met.3D
and demonstrates the use of 3-D and uncertainty visualization for weather forecasting
and for planning flight routes in the medium forecast range (three to seven days before
take-off).

1 Introduction

Weather forecasting during aircraft-based field campaigns requires the meteorologist to
explore large amounts of numerical weather prediction (NWP) data in a short period of
time. Atmospheric features relevant to a research flight have to be identified quickly, and
findings have to be communicated to colleagues. Furthermore, assessing the forecast's
uncertainty has become indispensable as flights frequently have to be planned several
days before take-off.

GMDD

8, 2161–2212, 2015

3-D visualization of ensemble weather forecasts – Part 2: Warm conveyor belts

M. Rautenhaus et al.

Title Page

Abstract

Introduction

Conclusions

References

Tables

Figures



Back

Close

Full Screen / Esc

Printer-friendly Version

Interactive Discussion



3-D visualization of ensemble weather forecasts – Part 2: Warm conveyor belts

M. Rautenhaus et al.

Title Page

Abstract

Introduction

Conclusions

References

Tables

Figures



Back

Close

Full Screen / Esc

Printer-friendly Version

Interactive Discussion



A challenging element in forecasting methodology is to create clear and intuitive visualizations that allow the meteorologist to perform these tasks in a timely manner. To advance forecasting techniques for research flight planning, this work presents a new approach using interactive three-dimensional (3-D) visualization of ensemble weather predictions (the latter a major source of information on forecast uncertainty, Gneiting and Raftery, 2005; Leutbecher and Palmer, 2008) to forecast warm conveyor belt (WCB) situations.

The article is the second part of a two-paper study. The first part (Rautenhaus et al., 2015, hereafter R15P1) introduces *Met.3D*, a tool providing interactive 3-D techniques for the visual exploration of ensemble weather prediction data. This article focuses on the specific application case of forecasting WCBs; strong, ascending, and often rain producing airstreams associated with mid-latitude weather systems (Browning and Roberts, 1994; Eckhardt et al., 2004; Pfahl et al., 2014). WCBs are an atmospheric feature that has been in the focus of several aircraft-based campaigns (Pomroy and Thorpe, 2000; Vaughan et al., 2003; Schäfler et al., 2014).

A recent campaign that targeted WCBs is T-NAWDEx-Falcon 2012 (THORPEX – North Atlantic Waveguide and Downstream Impact Experiment, hereafter TNF), which took place in October 2012 in southern Germany. Schäfler et al. (2014) describe the TNF flight planning process. WCBs (as well as other atmospheric features targeted by research flights) are of an inherently three-dimensional nature. However, despite the 3-D nature of the atmosphere, the forecasting and flight-planning tools employed during TNF relied on two-dimensional (2-D) visualization methods. This is a common property not only of campaign tools (Flatøy et al., 2000; Blakeslee et al., 2007; He et al., 2010; Rautenhaus et al., 2012) but also of meteorological workstations in general (Heizenrieder and Haucke, 2009; Russell et al., 2010). 3-D visualization methods are not commonly used in forecasting; only few reports on approaches using 3-D techniques have been published in the past two decades (Treinish and Rothfus, 1997; Koppert et al., 1998; McCaslin et al., 2000).

3-D visualization of ensemble weather forecasts – Part 2: Warm conveyor belts

M. Rautenhaus et al.

Title Page

Abstract

Introduction

Conclusions

References

Tables

Figures



Back

Close

Full Screen / Esc

Printer-friendly Version

Interactive Discussion



Similarly, ensemble predictions have, to the best of our knowledge, not been used extensively during aircraft-based campaigns. However, in particular the possibility to use ensembles to compute 3-D probability fields of the occurrence of features or events is valuable for flight planning. For the WCB case, a probability of WCB occurrence can be used to plan flight routes in regions in which the probability to encounter a WCB is at a maximum.

The work presented in this article is motivated by the questions of (1) how interactive 3-D visualization can be used to improve the exploration of 3-D features of interest to a flight campaign, and (2) how ensemble forecasts (in particular derived probabilities) can be used to improve research flight planning in the medium forecast range (that is, three to seven days before take-off). Our developments have been guided by a number of forecast questions that reflect the TNF requirements. They are repeated here from R15P1 for completeness:

- FQ-A: how will the large scale weather situation develop over the next week, and will conditions occur that favour WCB formation?
- FQ-B: how reliable are the weather predictions?
- FQ-C: where and when, in the medium forecast range and within the range of the aircraft, is a WCB most likely to occur?
- FQ-D: how reliable is the forecast of WCB occurrence?
- FQ-E: where will the WCB be located relative to cyclonic and dynamic features?

The technical basis for (FQ-A) and (FQ-B) is laid in R15P1. This article addresses (FQ-C) to (FQ-E) and presents a case study that demonstrates how the methods developed in both papers are applied to forecasting.

The paper is structured as follows. In Sect. 2, we propose a technique to compute 3-D probabilities of WCB occurrence. Our approach is put into relation to previous work in the field, and its integration into the Met.3D architecture is described. During TNF,

3-D visualization of ensemble weather forecasts – Part 2: Warm conveyor belts

M. Rautenhaus et al.

Title Page

Abstract

Introduction

Conclusions

References

Tables

Figures



Back

Close

Full Screen / Esc

Printer-friendly Version

Interactive Discussion



we followed the approach of Wernli and Davies (1997) and used Lagrangian particle trajectories computed on the forecast wind field to objectively detect WCB airstreams. Using wind forecasts from the European Centre for Medium Range Weather Forecasts (ECMWF) Ensemble Prediction System (ENS), trajectories were started from the atmospheric boundary layer (ABL) for each ensemble member. Those trajectories fulfilling a WCB criterion were gridded into 2-D grids and displayed as probability maps showing the occurrence of either or all of WCB inflow, ascent, and outflow. However, generalising this approach to three dimensions poses challenges, as discussed in Sect. 2. We present an adapted approach using domain-filling trajectories, which is more accurate, albeit computationally more expensive. In order to find the best method that is still computationally tractable in a forecast setting, both approaches are compared in Sect. 3. We analyse their sensitivity to the spatial resolution of the forecast wind fields and to the number and locations of the trajectory seeding points.

To facilitate quantitative interpretation of the obtained probabilities, we further propose a visual analysis method for cases in which only low probabilities of the occurrence of WCBs are encountered (Sect. 4). In such cases a flight often might not be planned due to the interpreted high uncertainty. However, low probability can have two causes. Either indeed only a small percentage of the ensemble members predict a WCB feature, or large spatial variation of the features in the individual ensemble members causes only marginal overlap and thus low probabilities. In the latter case the probability that a WCB will occur is actually much larger than suggested by the visualized probabilities. However, there is a large uncertainty in where it will occur. To help the user distinguish between these causes, we propose a method that identifies the contribution of individual members to a probability region.

After the introduction of all methods that are required to explore a forecast to answer questions (FQ-A) to (FQ-E), Sect. 5 revisits the TNF forecast case of 19 October 2012. The case study shows how the proposed 3-D ensemble visualization workflow is applied to campaign forecasting, and illustrates the use and added value of the presented methods.

The paper is concluded with a summary and discussion in Sect. 6.

2 Probability of warm conveyor belt occurrence

WCBs are Lagrangian airstreams in extratropical cyclones. They transport warm and moist air from the ABL in a cyclone's warm sector upward and poleward towards the tropopause. The inflow region in the lower troposphere typically extends over several hundred kilometres in diameter. WCB airmasses commonly ascend by about 500 to 600 hPa in 48 h, thereby covering horizontal distances of up to 2000 km (Wernli and Davies, 1997; Eckhardt et al., 2004). Due to the strong ascent, condensation leads to strong latent heat release and the formation of clouds and precipitation, making WCBs highly relevant for precipitation extremes in the extratropics (Pfahl et al., 2014). Once the airmasses reach jet level, an outflow region forms near the tropopause. This region is characterised by cirrus clouds that extend over several thousand kilometres along the jet stream. Readers interested in further detail are referred to Madonna et al. (2014), who give a comprehensive introduction to the field.

To plan a flight that allows aircraft measurements within a WCB, we are interested in the spatial and temporal distribution of WCB features in the ensemble forecast. As a summary measure of the uncertainty information, the probability of WCB occurrence, $p(\text{WCB})$, is of particular interest. It provides for a given location in 3-D space at a given time the probability of encountering a WCB airmass. To compute $p(\text{WCB})$ from an ensemble weather forecast, we first need to detect WCB features in the individual ensemble members. In early studies of Harrold (1973), Carlson (1980) and Browning (1986), conveyor belt airstreams have been identified by manual inspection of satellite imagery or by isentropic analysis. In more recent studies, WCBs are frequently detected from numerical weather and climate simulation output by using Lagrangian particle trajectories. This approach allows for an objective identification of the WCB structures.

For our work, we are interested in the specific ways trajectories are used in the literature to detect WCBs. In particular, this includes the spatial and temporal resolution

GMDD

8, 2161–2212, 2015

3-D visualization of ensemble weather forecasts – Part 2: Warm conveyor belts

M. Rautenhaus et al.

Title Page

Abstract

Introduction

Conclusions

References

Tables

Figures

◀

▶

◀

▶

Back

Close

Full Screen / Esc

Printer-friendly Version

Interactive Discussion



of the trajectories as well as the employed wind fields. In Sect. 2.1, we review literature on trajectory-based WCB detection. Our approach to derive 3-D fields of $p(\text{WCB})$ from the detected features is described in Sect. 2.2, and the integration of the method into Met.3D is topic of Sect. 2.3.

2.1 Review of trajectory-based WCB detection

Wernli and Davies (1997) have introduced the usage of Lagrangian particle trajectories to analyse the dynamics of extratropical cyclones. They use wind fields from the ECMWF global atmospheric model, interpolated (from a spherical truncation of T213) to a regular latitude/longitude grid of $0.75^\circ \times 0.75^\circ$ with 31 levels in the vertical and 6 h time resolution. Trajectories are started on every model grid point below 800 hPa (approx. 7 levels). A number of criteria are used to extract what they call “coherent ensembles of trajectories” (CET, a bundle of trajectories started at different locations; not to be confused with the meaning of “ensemble” in “ensemble forecasts”). Wernli and Davies show that nearly identical CETs are obtained by selecting trajectories that experience either a moisture decrease of 12 g kg^{-1} in 48 h or an ascent of more than 620 hPa in 48 h. In a subsequent article, Wernli (1997) applies the suggested method to the case study of Browning and Roberts (1994) and relates the obtained CETs to the WCB model.

Stohl (2001) and Eckhardt et al. (2004) compute climatologies of WCBs. Stohl (2001) seeds the trajectories on a $1^\circ \times 1^\circ$ grid in the horizontal and on two vertical levels at 500 and 1500 m a.s.l. He notes that the results of his climatology are sensitive to the WCB selection criterion, and settles for the – as he writes – “somewhat arbitrary” criterion of 8000 m in 48 h (the approximate time scale at which air flows through a single synoptic system). Similarly, Eckhardt et al. (2004) start trajectories on a $1^\circ \times 1^\circ$ grid at 500 m a.s.l. They note that “any criterion used for an automatic classification of WCBs is necessarily subjective”. In their work, trajectories travelling more than 10° eastward and 5° northward and ascending more than 60% of the average tropopause height within 48 h are classified as WCB trajectories.

3-D visualization of ensemble weather forecasts – Part 2: Warm conveyor belts

M. Rautenhaus et al.

Title Page

Abstract

Introduction

Conclusions

References

Tables

Figures

⏪

⏩

◀

▶

Back

Close

Full Screen / Esc

Printer-friendly Version

Interactive Discussion



of spherical geometry requires the computation of a very large number of trajectories. Yet, geometry that reflects the different scales (for example ellipses, cylinders or simple rectangular boxes) is difficult to motivate physically. Also, usage of large air parcels neglects potential deformation of the parcels by the wind field.

5 An approach not requiring any such assumptions is to use domain-filling trajectories (in the following referred to as *DF-T method*). Here, we first specify the grid topology for B . Next, as illustrated in Figs. 2b, c and 3, for every member and each grid point B_{kji}^m , a trajectory starting on B_{kji}^m is computed. This way, we can be certain that each B_{kji}^m is placed exactly on a trajectory and no assumptions about the shape of the particle volume need to be made. After applying a WCB selection criterion to the trajectories, the bits of the grid points from which WCB trajectories were started are set. However, the approach requires increased computational resources. Seeding points are now required on all tropospheric layers and hence a larger number of trajectories is required. Also, trajectories additionally have to be computed backward in time to also capture those situations in which a WCB trajectory passes its seeding point in the ascent or outflow phase. Step (1.) in the method description above is hence extended to also integrate the trajectories backward in time for Δt hours from time t .

15 In Sect. 3, we compare four DF-T and ABL-T setups with varying grid topology with respect to obtained $p(\text{WCB})$ and to computational demand. The comparison allows to find a setup well suited for usage in campaign forecasting.

2.3 Implementation

25 Trajectories computed with LAGRANTO are stored in NetCDF files. Trajectory selection and the computation of $p(\text{WCB})$ take place in Met.3D and have been implemented in a number of modules in the data processing pipeline (Sect. 4.2 of R15P1). Figure 4 shows an example setup. Separate modules are responsible for reading trajectory data from disk, filtering the data according to the selection criterion, gridding and probability computation. This architecture allows modules to be exchanged when, for example,

3-D visualization of ensemble weather forecasts – Part 2: Warm conveyor belts

M. Rautenhaus et al.

Title Page

Abstract

Introduction

Conclusions

References

Tables

Figures



Back

Close

Full Screen / Esc

Printer-friendly Version

Interactive Discussion



data from a different trajectory model should be read or a different selection criterion should be applied.

Intermediate results in the pipeline are cached by a memory manager (R15P1). This increases the interactivity of the system with respect to changing the selection parameters Δp and Δt . As an example, Fig. 3 shows results of selecting domain-filling trajectories that ascend more than 500 hPa in 48 h (a–c) and more than 600 hPa in 48 h (d–f). Note how the 30 % isosurface of $p(\text{WCB})$ over the English Channel almost vanishes with 600 hPa filtering (Fig. 3f).

To select trajectories according to the ascent criterion, the maximum pressure change occurring within a trajectory over the time interval Δt is required. For the grid resolution used here, the data volume of the trajectories of all members amounts to multiple GB per timestep if stored in binary NetCDF format (approximately 2.4 GB for 1° horizontal resolution with 62 levels in the vertical and approximately 38 GB if the horizontal resolution is increased to 0.25°). Reading the data from disk and performing the selection can hence be slow. We thus make use of the fact that the only information required to compute the probabilities is whether the trajectory started from a grid point fulfils the selection criterion. The data volume that needs to be loaded can be largely reduced by precomputing the maximum pressure change Δp for a range of time intervals Δt . Now, for a given Δt , only the maximum Δp for each trajectory (= grid point) needs to be read. The selection process is reduced to comparing each trajectory's Δp to the given threshold value. This way, we are able to provide an interactively adjustable selection criterion to the user.

3 Choice of $p(\text{WCB})$ method and grid resolution for forecasting

To use a $p(\text{WCB})$ method for forecasting during a campaign, a number of criteria need to be fulfilled:

GMDD

8, 2161–2212, 2015

3-D visualization of ensemble weather forecasts – Part 2: Warm conveyor belts

M. Rautenhaus et al.

Title Page

Abstract

Introduction

Conclusions

References

Tables

Figures

◀

▶

◀

▶

Back

Close

Full Screen / Esc

Printer-friendly Version

Interactive Discussion



3-D visualization of ensemble weather forecasts – Part 2: Warm conveyor belts

M. Rautenhaus et al.

Title Page

Abstract

Introduction

Conclusions

References

Tables

Figures

⏪

⏩

◀

▶

Back

Close

Full Screen / Esc

Printer-friendly Version

Interactive Discussion



- a. The trajectories need to be computed in a short period of time (for our application this is preferably less than one hour), so that results are available soon after the forecast wind fields become available from ECMWF,
- b. the amount of trajectory data needs to be small enough to be handled interactively in Met.3D,
- c. the resolution needs to be fine enough to capture the important features that are present in a “best possible” forecast.

3.1 Evaluated setups

We evaluate four different setups with respect to the given criteria:

- S1. As the “best possible” $p(\text{WCB})$ forecast, we use a DF-T setup with trajectories computed on the ECMWF ENS wind fields at the highest available resolution (T639L62, horizontally interpolated to a regular grid of $0.25^\circ \times 0.25^\circ$ in latitude and longitude, with 62 terrain-following levels in the vertical). Care must be taken with respect to the choice of the B^m and $p(\text{WCB})$ grids. A straightforward choice is to use the ECMWF grid on which the wind fields are available. However, the vertical position of the grid points on ECMWF model levels depends on the surface pressure field (Untch and Hortal, 2004, also cf. R15P1 Sect. 4.1), which varies between ensemble members. Hence, if the individual members’ wind grids are used for the B^m , the problem described in R15P1, Sect. 5 arises: the grid points are located at different vertical positions across the ensemble, and hence an error is introduced when computing the probability. To avoid this problem while staying as close as possible to the ECMWF grid, we use the grid defined by the ensemble minimum surface pressure for the B^m of all members. The minimum surface pressure is chosen to ensure that all grid points are located above the surface (if the mean surface pressure is used, grid points in the lowest levels can be located below the surface in some members).

though. For trajectory integration, the same forecast data as in (S2.) and (S3.) are used.

For all trajectory computations, LAGRANTO is driven with ECMWF ENS forecast data at six-hour timesteps. The model internally uses a 30 min timestep for the integration, trajectory positions are output at six-hour intervals.

3.2 Setup comparison

In terms of computational resources, setup (S1.) is the most demanding configuration. On our test system (six-core Intel Xeon running at 2.67 GHz; 24 GB RAM; 512 GB solid state drive), the computation of the trajectories of a single timestep takes about 50 CPU minutes per member. The data output for a timestep of all members, stored in binary NetCDF format, amounts to approximately 38 GB. While such simulations are feasible for research settings, they are not suited for forecasting. For setups (S2.) and (S3.), the number of trajectories decrease by a factor of 16. The time required to compute the trajectories reduces to about three CPU minutes per timestep and member, about 2.4 GB of trajectory data are produced per timestep for the entire ensemble. With the current ENS size of 50 members, this setting is feasible for forecasting if a small compute cluster is available. For setup (S4.), the time further reduces to about one CPU minute and data volume reduces to approximately one GB.

In Fig. 5, the three DF-T setups are compared by means of four typical visualizations of the Met.3D workflow: (a) the volume rendering of p (WCB) isosurfaces already used in Fig. 3c, (b) a volume rendering of WCB features in the the control forecast, (c) a horizontal section at 410 hPa through the ascent region associated with precipitation, and (d) a horizontal section through the inflow region at 950 hPa. The TNF forecast case of 19 October 2012 that already served for the examples in R15P1 is used. The main features (cf. Fig. 1 in R15P1: inflow over the Mediterranean Sea, ascent over the English Channel and Southern England, outflow over Scandinavia and Russia, as well as a strong ascent associated with former Hurricane Rafael over the North Atlantic) are

3-D visualization of ensemble weather forecasts – Part 2: Warm conveyor belts

M. Rautenhaus et al.

Title Page

Abstract

Introduction

Conclusions

References

Tables

Figures



Back

Close

Full Screen / Esc

Printer-friendly Version

Interactive Discussion



4 Probability region contribution

The methods introduced so far allow to visualize the computed $p(\text{WCB})$ fields and to find regions in which the occurrence of a WCB is most likely. However, it remains an open question how the magnitudes of the displayed probabilities should be interpreted.

5 A distinct property of the examples presented in Sect. 3 are relatively low probabilities. For instance, in Fig. 3c maximum values only reach about 30 %. As mentioned in the introduction, such low magnitudes can have two causes: either indeed only 30 % of all ensemble members predict the WCB event, or large spatial variation of the features in the individual members causes only marginal overlap and thus low probabilities. Also,
10 noise in the individual binary volumes can cause empty grid cells in the features and decrease probability values. Interpreting the data correctly and being able to distinguish between these causes is very important for making decisions on potential flight routes.

The issue can be approached by looking at the individual ensemble members, as illustrated in Fig. 7. While due to limited print space Fig. 7 only shows a small selection
15 of members, we indeed find that much more than 30 % of the members predict a WCB feature. However, it is difficult for a human user to remember how many of the 51 members showed a WCB feature. Visualizing the WCB features of all members in a single view (Fig. 7f) results in massive clutter and, thus, does not reveal insight.

We are interested in the following information: given a region bounded by a probability isosurface, how many individual ensemble members predict a WCB feature that overlaps with this region and that, thus, contributes to the probability value at any of the grid points inside the isosurface? To determine this number of members, we propose a method that applies region growing to identify the grid points inside the isosurface, then uses the members' binary grids B^m to determine which members have
25 contributed. To efficiently make use of the B^m , we condense the binary grids into bit-

on a six-core Intel Xeon running at 2.67 GHz) and a sampling step size of 0.1, the top row isosurface visualization in Figs. 5 and 6 require on average 361 ms for setup (S2.) and 102 ms for (S3.).

3-D visualization of ensemble weather forecasts – Part 2: Warm conveyor belts

M. Rautenhaus et al.

Title Page

Abstract

Introduction

Conclusions

References

Tables

Figures



Back

Close

Full Screen / Esc

Printer-friendly Version

Interactive Discussion



fields that are stored together with the probability volume. For the current example and for the 51 members of the ECMWF ensemble, each grid point $p(\text{WCB})_{kji}$ is augmented by a bitfield stored in a 64-bit integer variable (one bit for each member). The bitfields are generated during evaluation of the probability criterion (in this case, step (3.) in Sect. 2).

Figure 8 illustrates the approach. In a hypothetical ensemble of ten members, nine members predict a WCB feature (coloured bars). However, the maximum probability value that occurs is 30 % (red region). To determine the contribution to the region, the algorithm scans the volume for grid points exceeding the 30 % value. Starting from the first identified point, a region growing algorithm determines all grid points belonging to the red region. Combining the bitfields of the identified points with a bitwise “or”-operation reveals that in total, members 1, 2, 3, 4, 5, 6, 8 and 9, thus 80 % of the ensemble, contribute to the region. We hence know that much more than 30 % of all members predict a WCB. The information is stored for each of the identified grid points in a separate data field, the *contribution volume*. It needs to be recomputed every time the probability isovalue changes. For example, applying the algorithm to the white 10 % region in Fig. 8 yields a contribution of 90 %.

The contribution volume can be used in visualizations of $p(\text{WCB})$ to colour a probability isosurface according to the number of members that contribute. Figure 9 shows the application of the method to the WCB forecast from Fig. 3c, setup (S3.). Whenever an isosurface point is identified and visualized (cf. R15P1, Sect. 4.3, for the employed raycasting algorithm), the eight data points that enclose the isosurface position are sampled. Since the isosurface value is interpolated from these eight points, at least the point with the maximum probability value is located inside the isosurface, and the point with the lowest value is located outside the isosurface (otherwise no crossing could be found between the points). Thus, by sampling the contribution volume at the grid point with the maximum value (and exploiting the fact that all grid points of a contiguous structure in the contribution volume carry the same value) the number (or percentage) of contributing members can be obtained. Indeed, Fig. 9c shows that about 85 % of the

GMDD

8, 2161–2212, 2015

3-D visualization of ensemble weather forecasts – Part 2: Warm conveyor belts

M. Rautenhaus et al.

Title Page

Abstract

Introduction

Conclusions

References

Tables

Figures



Back

Close

Full Screen / Esc

Printer-friendly Version

Interactive Discussion



static figures, as well as additional content, in animated form. To compute $p(\text{WCB})$, setup (S3.) from Sect. 3 is used.

Assume the forecast activities to take place on Monday, 15 October 2012. The ensemble and deterministic predictions initialised at 00:00 UTC on that day, as well as the preceding model runs, are available to the forecaster (in the following, we abbreviate forecasts initialisation and valid times as IT15/00Z, VT19/12Z, etc.). We are interested in areas that favour WCB development in Central Europe, being reachable with the DLR Falcon aircraft from the campaign base in Oberpfaffenhofen, Southern Germany. Due to requirements from air traffic authorities, potential flight routes need to be announced at least three days in advance of a flight. Hence, our aim is to explore the atmospheric situation in order to evaluate suitable flight conditions towards the end of the week.

5.1 Weather situation

Our first step is to study the large scale weather situation in the deterministic high-resolution forecast to analyse whether a promising synoptic situation will develop (FQ-A). The upper level flow is of particular interest. WCBs frequently occur on the leading edge (i.e. downstream) of troughs (where low pressure systems develop), and WCB outflow is often associated with jet streaks. We start with a Met.3D configuration featuring three views: a horizontal section of wind speed and geopotential height (initially placed at jet stream level at 250 hPa), 3-D isosurfaces of wind speed, and 3-D isosurfaces of cloud cover. We explore the time period from Wednesday, 17 October, to Sunday, 21 October. Figure 10 shows screenshots of the individual views at three selected timesteps. To capture the 3-D spatial structure of the jet, the isosurfaces of wind speed are visualized at 30 and 50 ms^{-1} . Cloud cover is visualized by isosurfaces at 0.2 and 0.7, the latter coloured by elevation. Both 3-D views contain contour lines at surface level showing the mean sea level pressure. The video shows the Met.3D window with the full time animation.

GMDD

8, 2161–2212, 2015

3-D visualization of ensemble weather forecasts – Part 2: Warm conveyor belts

M. Rautenhaus et al.

Title Page

Abstract

Introduction

Conclusions

References

Tables

Figures



Back

Close

Full Screen / Esc

Printer-friendly Version

Interactive Discussion



covering Western France to Southern England, the location in space and time of the WCB ascent is still uncertain in the IT15/00Z forecast.

To judge the strength of the predicted ascent, we modify the trajectory selection criterion. Figure 14 (video at 03:38 min) shows how the predicted $p(\text{WCB})$ changes with $\Delta\rho$. By decreasing $\Delta\rho$ (Fig. 14a), we can confirm a high likelihood of ascending airmasses in the region of interest³; the probability increases with decreasing $\Delta\rho$. Increasing $\Delta\rho$ (Fig. 14b) reduces the predicted probabilities. However, the location of the maximum remains at the same position. The region in which high probabilities for ascending airmasses are forecast is hence also the region in which the strongest updrafts occur.

5.3 WCB characteristics

The next goal is to characterise the predicted ascent with respect to related atmospheric processes (FQ-E). We take a closer look at the WCB trajectories of the ensemble control run and visualize the trajectory particle positions at single timesteps. Animation over the timesteps of the trajectories computed forward and backward from VT19/18Z reveals that the air that on VT19/18Z has ascended to the region over the Channel originates from the ABL over the Western Mediterranean Sea and Northwestern Africa around VT18/18Z (Fig. 15a, video at 04:10 min). It is lifted over Spain in the early hours of 19 October and over the course of the day continues its ascent over Western France, the Channel and Southern England (Fig. 15b, c). By vertically shifting a horizontal section of geopotential height and equivalent potential temperature of the deterministic forecast on VT18/18Z (similar to the ensemble control but chosen here for its added detail), we discover a cyclone over the Northern British Isles, and a weaker surface low located on the west coast of France (Fig. 15d, video at 04:28 min). South

³Note that the normal curves are again advantageous for this interaction as they allow to visually track the location and magnitude of maximum probabilities despite the changing magnitudes.

3-D visualization of ensemble weather forecasts – Part 2: Warm conveyor belts

M. Rautenhaus et al.

Title Page

Abstract

Introduction

Conclusions

References

Tables

Figures



Back

Close

Full Screen / Esc

Printer-friendly Version

Interactive Discussion



3-D visualization of ensemble weather forecasts – Part 2: Warm conveyor belts

M. Rautenhaus et al.

Title Page

Abstract

Introduction

Conclusions

References

Tables

Figures



Back

Close

Full Screen / Esc

Printer-friendly Version

Interactive Discussion



of Spain, warm and moist air (high equivalent potential temperature) is advected northward. This air mass represents the WCB inflow region; it is subsequently lifted by the WCB. In contrast, on the rear side of the trough, colder and drier air masses over the East Atlantic are transported southward to Spain. Over the following 24 h, the cyclone over the British Isles remains stationary, the weaker surface low moves towards Norway (Fig. 15e, f, video at 04:52 min). Animation over the ensemble members reveals that most other members predict similar ascents originating from the Western Mediterranean Sea and Northwestern Africa. Figure 16 reproduces the visualization of Fig. 15c for the members shown in Fig. 13b, c, and d. The trajectory particles that represent the WCB air masses are lifted along similar paths. However, the temporal evolution of the WCBs differs in the members. On VT19/18Z, the air masses are at different stages of their ascent.

Figure 17 shows vertical sections of potential vorticity (PV) and cloud cover of the VT19/18Z deterministic forecast (animated in the video at 05:19 min). The dynamic tropopause, as indicated by the 2-PVU-surface, folds along the trough (Fig. 17a). On the rear side of the trough, dry stratospheric air is transported downward. On its leading edge, the tropopause is elevated where it transitions into the anticyclonic region over Central Europe. Between 700 and 500 hPa, increased values of PV indicate regions of diabatic PV production. They coincide with the cold front that can be identified from the strong gradient in equivalent potential temperature (dense contour lines below the clouds in Fig. 17b). The cold front tilts westward with height, matching the tilted structure of the p (WCB) isosurface described in the previous section. Ahead (east) of the front, predicted cloud cover largely coincides with the location of the WCB. Overall, the situation resembles the classic conceptual WCB model (Browning, 1986). The WCB outflow predicted over the North Sea on VT20/00Z is related to lower PV values aloft. This is consistent with predicted ice water and cloud cover in this region (not shown).

5.4 Potential flight segments

Given the findings from the previous subsections, we interpret the $p(\text{WCB})$ maximum as the most likely location for the predicted WCB event and draft potential flight segments. Figure 18 shows the corresponding Met.3D configuration. For VT19/12Z and VT19/18Z, we slide a horizontal section through the $p(\text{WCB})$ volume to determine precise locations of the maxima (video at 05:42 min). On VT19/12Z, maximum probabilities are located above the Pyrenees at low levels, in the Bordeaux area between 700 and 600 hPa, and south of Brittany around 400 hPa. Six hours later, the maximum is most prominent above Southern England at altitudes around 400 hPa. A vertical section is used to explore potential flight segments. It allows to estimate at which elevation a flight should take place, and, by moving the section, to quickly assess how spatially relocating the leg will impact the expected measurements. In the given case, the 2-D sections suggest flight legs on VT19/12Z over France at elevations between 800 and 600 hPa (WCB ascent) and on VT19/18Z over Southern England at elevations around 400 hPa (WCB outflow)⁴.

However, given the uncertainty in the temporal evolution of the WCB (previous section), we need to carefully monitor developments in subsequent forecast runs. Figure 19 (video at 07:38 min) shows the predictions for VT19/18Z for forecast runs subsequent to the IT15/00Z run. Over the next two days, the ensemble predictions converge toward higher $p(\text{WCB})$ over the English Channel and Southern England. The elevation of the predicted maximum in $p(\text{WCB})$ remains approximately constant. Indeed, the research flights conducted during TNF showed that the targeted WCB occurred as predicted (Schäfler et al., 2014).

⁴During TNF, we did not have the vertical $p(\text{WCB})$ information available. We placed the flight along a horizontally pre-defined flight leg over France which appeared to fit well with the 2-D $p(\text{WCB})$ product. We were only able to guess at which altitudes we should fly. In fact, from the 3-D $p(\text{WCB})$ data we find that the flight should rather have been planned south of the pre-defined flight leg.

3-D visualization of ensemble weather forecasts – Part 2: Warm conveyor belts

M. Rautenhaus et al.

Title Page

Abstract

Introduction

Conclusions

References

Tables

Figures



Back

Close

Full Screen / Esc

Printer-friendly Version

Interactive Discussion



6 Conclusions

Motivated by the forecast requirements of the T-NAWDEX-Falcon 2012 campaign, we have demonstrated the feasibility of applying interactive 3-D ensemble visualization to forecasting warm conveyor belt situations during aircraft-based field campaigns. The article extends our work presented in R15P1, in which we have introduced the new open-source 3-D ensemble visualization tool Met.3D. In the present paper, we have proposed methods to compute and to visually analyse 3-D probabilities of WCB occurrence. The techniques have been integrated into Met.3D and are part of the released version 1.0 (see R15P1, Sect. 6, for information on code availability). A case study, revisiting a forecast case that occurred during T-NAWDEX-Falcon, has demonstrated how the methods introduced in the two papers can be used for practical forecasting.

Following the literature, our methods detect WCBs by means of Lagrangian particle trajectories. By computing trajectories for each member of the ECMWF ensemble forecast, a distribution of WCB features is obtained from which probabilities of occurrence can be derived. We have discussed different approaches to trajectory seeding and gridding, and have shown that probabilities derived from trajectories computed at a horizontal resolution of 1° in latitude and longitude capture the same WCB structures as trajectories computed at a higher resolution of 0.25° . A proposed visual analysis method supports the interpretation of the probability fields. The method facilitates fast visual estimation of the number of ensemble members that forecast a WCB feature in a region of interest bounded by a probability isosurface. In particular for situations in which the magnitude of observed probabilities is low, the method helps to distinguish the case in which only few members predict a WCB but at approximately the same location, from the case in which many members predict a WCB but the spatial variation is high. The method can be applied to probabilities of other features as well.

With Met.3D and the proposed WCB methods, we are now able to analyse ensemble prediction data in a way previously impossible. Three of us (M. Rautenhaus, C. M. Grams, A. Schäfler) have actively been involved in forecasting during aircraft-

GMDD

8, 2161–2212, 2015

3-D visualization of ensemble weather forecasts – Part 2: Warm conveyor belts

M. Rautenhaus et al.

Title Page

Abstract

Introduction

Conclusions

References

Tables

Figures



Back

Close

Full Screen / Esc

Printer-friendly Version

Interactive Discussion



based field campaigns. With respect to the case study and our experience in research flight planning, we note a few conclusions from our work, reflecting the authors' opinions.

1. Combination of 2-D and 3-D visualization methods gives a more complete picture of the forecast atmosphere. 3-D elements can depict different aspects of the data than horizontal and vertical 2-D sections alone. For example, usage of isosurfaces and normal curves allows for very fast initial judgement of the predicted WCB situation. However, we would not want to abandon the familiar 2-D sections; for many tasks (obtaining quantitative information, visualizing multiple forecast parameters in the same plot, analysing the vertical structure of the atmosphere along a flight segment) they are superior to 3-D methods. If 3-D visualization is used, achieving good spatial perception is important, as we have discussed in R15P1.

Furthermore, while we think that 3-D visualization helps to understand the atmospheric situation in many cases, it does not work equally well for all forecast variables. For the isosurfaces of wind speed and WCB probability used in the case study, 3-D visualization is well suited. For variables that highly fluctuate in space (as is often the case for variables depending on moisture, such as relative humidity), isosurfaces are problematic. For these cases, additional methods that help the user focus on the regions and features of interest will need to be developed.

2. One of the primary advantages of Met.3D is the high pace at which a forecast can be explored. Interactivity, the possibility for the user to change a parameter that affects the visualization and to receive immediate visual feedback, is key to this property. It facilitates the very fast analysis of static scenes (moving the camera to explore spatial structure of a feature, moving a vertical axis), of dynamic processes (animation over time), of uncertainty (animation over the ensemble, comparison of different forecast base times), and of sensitivity (changing a parameter that affects a displayed statistical quantity).

3-D visualization of ensemble weather forecasts – Part 2: Warm conveyor belts

M. Rautenhaus et al.

Title Page

Abstract

Introduction

Conclusions

References

Tables

Figures



Back

Close

Full Screen / Esc

Printer-friendly Version

Interactive Discussion



3-D visualization of ensemble weather forecasts – Part 2: Warm conveyor belts

M. Rautenhaus et al.

Title Page	
Abstract	Introduction
Conclusions	References
Tables	Figures
⏪	⏩
◀	▶
Back	Close
Full Screen / Esc	
Printer-friendly Version	
Interactive Discussion	



However, we find that while interactivity enables the user to quickly visualize a large amount of data, the user is also confronted with many more images than he would be if he were restricted to, for example, a limited number of horizontal sections. Here, as Trafton and Hoffman (2007) suggest, a virtual “sketchpad” that captures elements discovered by the forecaster and that allows him to represent his “mental model” of the atmosphere would be useful. The sketchpad could also be used to communicate the findings to colleagues, a common challenge during campaigns.

3. Our methodology to predict probabilities of WCB occurrence illustrates challenges of feature-based approaches to analyse ensemble data. Our region contribution approach helps to interpret the derived probabilities, however, further work will be useful. For example, we would like to automatically obtain information about how features in different members correspond to each other: do other members predict the same situation but shifted in space or in time? Such information would allow to identify different scenarios forecast by the ensemble, and uncertainty could be differentiated with respect to space and time. Detection and visualization of further 3-D cyclonic features would also be very useful. For a single member we could see, for example, at a glance which WCB transports which airmass along which route, driven by which cyclone and in relation to which front and jet stream. How to meaningfully visualize such features for an entire ensemble to depict their uncertainty is an open research question.
4. A drawback of the Met.3D visualization approach is that since it uses the complete ensemble dataset, interactive usage requires the forecast data to be available on the local hard drive. For field campaigns based at remote locations, this is not feasible. In these cases, web based approaches such as DLR’s Mission Support System (Rautenhaus et al., 2012) might be the better choice. Alternatively, dedicated ensemble compression schemes might enable more efficient remote han-

ding, or remote visualization solutions such as VirtualGL⁵ could be used to locate data and visualization system at the same site while allowing users to explore the data remotely using a modest internet connection.

We will actively use and further evaluate our developments during upcoming field campaigns, including a future NAWDEX campaign scheduled for 2016. It will again target WCBs. We also intend to continue our work on trajectory-based ensemble analysis. For example, trajectories can be applied to detect further Lagrangian features as well. Different selection criteria can, for instance, reveal airmasses that have undergone specific physical processes. In this respect, more complex selection algorithms and the visualization of combined probabilities of multiple features will be challenging.

Considering the ever increasing data volume generated by ensemble weather prediction systems, effective and intuitive visualization methods are and will be important to weather forecasting. The atmosphere is three-dimensional, and while we need to conduct user studies to formally prove the added value through 3-D visualization, in our opinion forecast analysis can be made much more intuitive by using interactive 3-D methods, thus decreasing the time a meteorologist needs to analyse a forecast dataset.

The Supplement related to this article is available online at [doi:10.5194/gmdd-8-2161-2015-supplement](https://doi.org/10.5194/gmdd-8-2161-2015-supplement).

Acknowledgements. Access to ECMWF prediction data has been kindly provided in the context of the ECMWF special project “Support Tool for HALO Missions”. This work was supported by the European Union under the ERC Advanced Grant 291372 – SaferVis – Uncertainty Visualization for Reliable Data Discovery. M. Rautenhaus was supported by a grant from Ev. Studienwerk Villigst e.V. C. M. Grams and A. Schäfler were supported by the German Research Foundation (DFG) as part of the research unit PANDOWAE (FOR896).

⁵<http://www.virtualgl.org>

3-D visualization of ensemble weather forecasts – Part 2: Warm conveyor belts

M. Rautenhaus et al.

Title Page

Abstract

Introduction

Conclusions

References

Tables

Figures



Back

Close

Full Screen / Esc

Printer-friendly Version

Interactive Discussion



3-D visualization of ensemble weather forecasts – Part 2: Warm conveyor belts

M. Rautenhaus et al.

Title Page

Abstract

Introduction

Conclusions

References

Tables

Figures

◀

▶

◀

▶

Back

Close

Full Screen / Esc

Printer-friendly Version

Interactive Discussion



- Trafton, J. G. and Hoffman, R. R.: Computer-aided visualization in meteorology, in: Expertise Out of Context: Proceedings of the Sixth International Conference on Naturalistic Decision Making, edited by: Hoffman, R. R., Chap. 15, Psychology Press, 337–357, 2007. 2189
- 5 Treinish, L. A. and Rothfus, L. P.: Three-dimensional visualization for support of operational forecasting at the 1996 Centennial Olympic Games, in: Proceedings of the 13th IIPS Conference, 2–7 February 1997, Long Beach, CA, 2–8, 1997. 2163
- Untch, A. and Hortal, M.: A finite-element scheme for the vertical discretization of the semi-Lagrangian version of the ECMWF forecast model, Q. J. Roy. Meteor. Soc., 130, 1505–1530, 2004. 2173
- 10 Vaughan, G., Garland, W. E., Dewey, K. J., and Gerbig, C.: Aircraft measurements of a warm conveyor belt – a case study, J. Atmos. Chem., 46, 117–129, 2003. 2163
- Wallace, J. M. and Hobbs, P. V.: Atmospheric Science: An Introductory Survey, Academic Press, 2 Edn., Amsterdam, 2006. 2174
- Wernli, H.: A Lagrangian-based analysis of extratropical cyclones. II: A detailed case-study, Q. J. Roy. Meteor. Soc., 123, 1677–1706, 1997. 2167
- 15 Wernli, H. and Davies, H. C.: A Lagrangian-based analysis of extratropical cyclones. I: The method and some applications, Q. J. Roy. Meteor. Soc., 123, 467–489, 1997. 2165, 2166, 2167, 2168

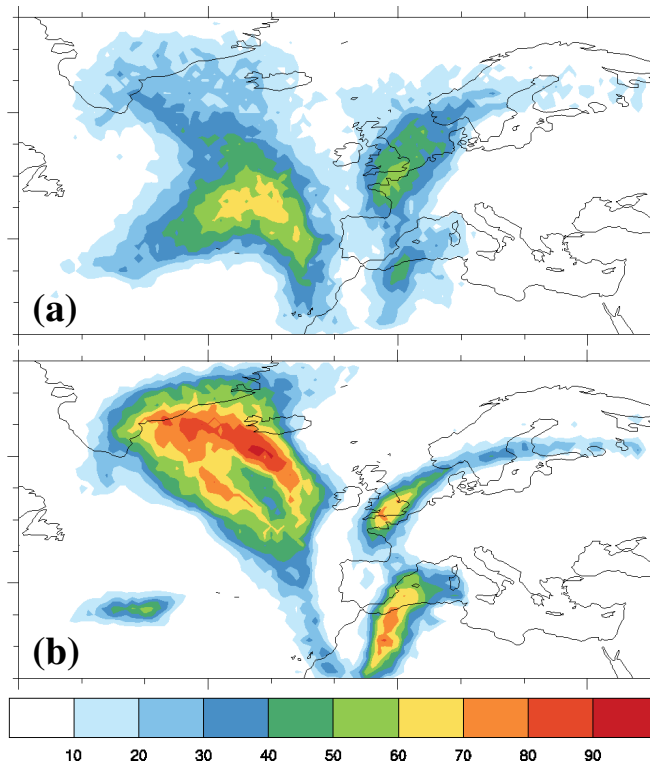


Figure 1. Total column probability of WCB occurrence (%), as available during TNF. Probabilities are computed from ABL-started trajectories filtered for an ascent of 500 hPa in 48 h. Forecasts from **(a)** 00:00 UTC on 15 October 2012 and from **(b)** 00:00 UTC on 17 October 2012, both valid at 18:00 UTC on 19 October 2012. Compare to Fig. 3 in Schäfler et al. (2014).

3-D visualization of ensemble weather forecasts – Part 2: Warm conveyor belts

M. Rautenhaus et al.

Title Page

Abstract

Introduction

Conclusions

References

Tables

Figures

◀

▶

◀

▶

Back

Close

Full Screen / Esc

Printer-friendly Version

Interactive Discussion



3-D visualization of ensemble weather forecasts – Part 2: Warm conveyor belts

M. Rautenhaus et al.

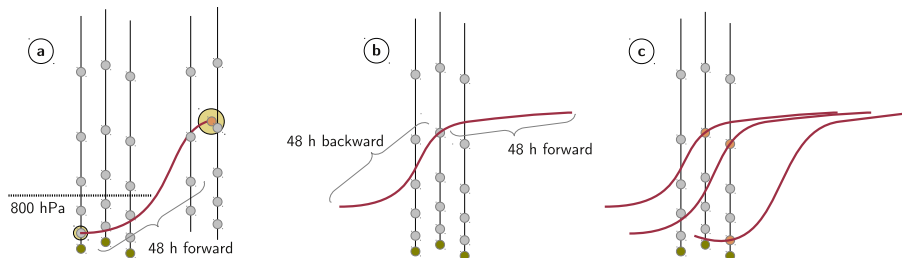


Figure 2. Methods to compute p (WCB). **(a)** ABL-T method using trajectories started in the atmospheric boundary layer and integrated 48 h forward in time. To get 3-D gridded information on WCB location, an air parcel volume needs to be assumed for each particle so that grid points overlapping with the volume can be determined. **(b)** DF-T method using domain-filling trajectories started from every grid point of the p (WCB) grid and integrated both 48 h forward and backward in time. No volume has to be assumed as the WCB trajectories are located exactly on grid points **(c)**.

Title Page

Abstract

Introduction

Conclusions

References

Tables

Figures

◀

▶

◀

▶

Back

Close

Full Screen / Esc

Printer-friendly Version

Interactive Discussion



3-D visualization of ensemble weather forecasts – Part 2: Warm conveyor belts

M. Rautenhaus et al.

Title Page

Abstract

Introduction

Conclusions

References

Tables

Figures



Back

Close

Full Screen / Esc

Printer-friendly Version

Interactive Discussion

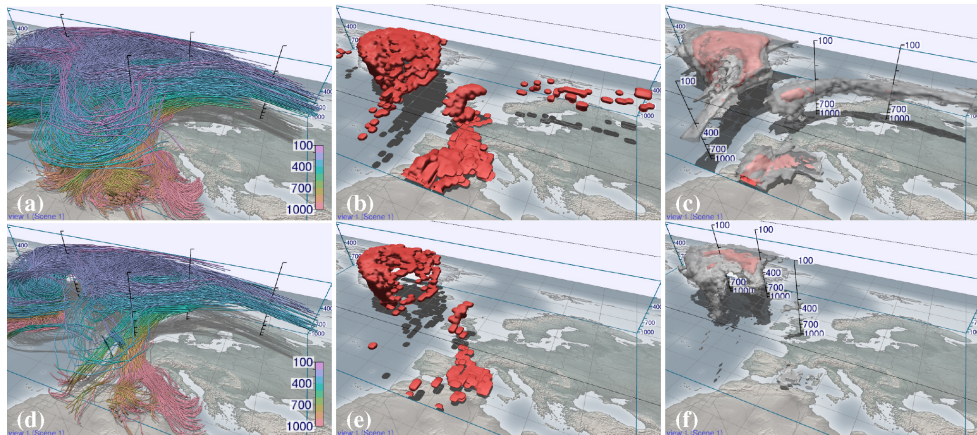


Figure 3. Deriving $p(\text{WCB})$ with DF-T setup (S3). **(a, d)** Trajectories of the control forecast started at 18:00 UTC on 19 October 2012 (forecast of 17 October, 00:00 UTC) integrated forward and backward in time for 48 h each. Trajectories are filtered according to an ascent of 500 **(a–c)** and 600 hPa **(d–f)** in 48 h. Colour encodes altitude (hPa). **(b, e)** Gridded start positions of the selected trajectories. **(c, f)** Probability of WCB occurrence derived from all 51 members of the ensemble. The red isosurface shows 30 % probability, the white isosurface 10 % probability.

3-D visualization of ensemble weather forecasts – Part 2: Warm conveyor belts

M. Rautenhaus et al.

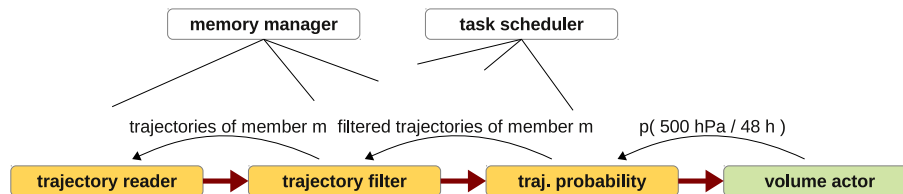


Figure 4. Sample pipeline to visualize WCB probability. A request for the probability of occurrence of trajectories triggers further requests up the pipeline. Intermediate results are cached by the memory manger. Compare to Fig. 10 in R15P1.

Title Page

Abstract

Introduction

Conclusions

References

Tables

Figures

⏪

⏩

◀

▶

Back

Close

Full Screen / Esc

Printer-friendly Version

Interactive Discussion



3-D visualization of ensemble weather forecasts – Part 2: Warm conveyor belts

M. Rautenhaus et al.

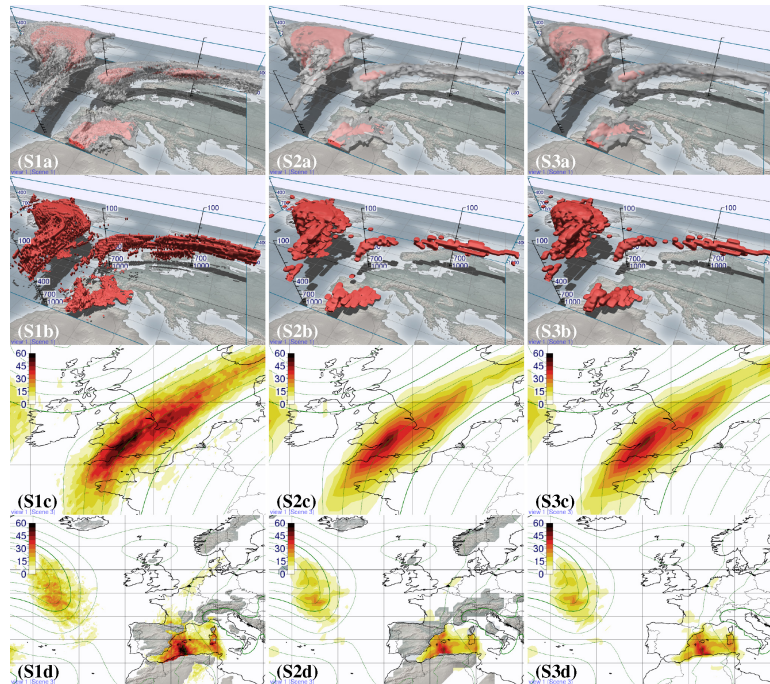


Figure 5. Comparison of DF-T setups to compute $p(\text{WCB})$. Same forecast as in Fig. 3. The selection criterion is set to 500 hPa in 48 h. (S1.) $0.25^\circ \times 0.25^\circ$ with 62 vertical hybrid levels defined by the ensemble minimum surface pressure; (S2.) as (S1.) but with $1^\circ \times 1^\circ$ horizontal resolution; (S3.) as (S2.) but defined by a constant surface pressure of 1000 hPa. **(a)** Volume rendering of $p(\text{WCB})$ (red isosurface shows 30 % probability, white isosurface 10 % probability); **(b)** volume rendering of a single member (member 12); **(c)** horizontal section of $p(\text{WCB})$ at 410 hPa; **(d)** horizontal section at 950 hPa. Green contour lines show ensemble mean geopotential height.

Title Page

Abstract

Introduction

Conclusions

References

Tables

Figures

⏪

⏩

◀

▶

Back

Close

Full Screen / Esc

Printer-friendly Version

Interactive Discussion



3-D visualization of ensemble weather forecasts – Part 2: Warm conveyor belts

M. Rautenhaus et al.

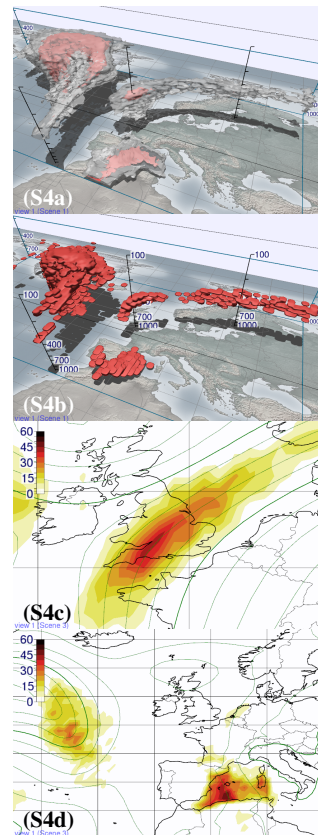


Figure 6. Same as Fig. 5, but for the ABL-T setup (S4.) with $1^\circ \times 1^\circ$ horizontal resolution and a regular vertical grid with a grid spacing of 10 hPa.

[Title Page](#)[Abstract](#)[Introduction](#)[Conclusions](#)[References](#)[Tables](#)[Figures](#)[⏪](#)[⏩](#)[◀](#)[▶](#)[Back](#)[Close](#)[Full Screen / Esc](#)[Printer-friendly Version](#)[Interactive Discussion](#)

3-D visualization of ensemble weather forecasts – Part 2: Warm conveyor belts

M. Rautenhaus et al.

Title Page

Abstract

Introduction

Conclusions

References

Tables

Figures

⏪

⏩

◀

▶

Back

Close

Full Screen / Esc

Printer-friendly Version

Interactive Discussion

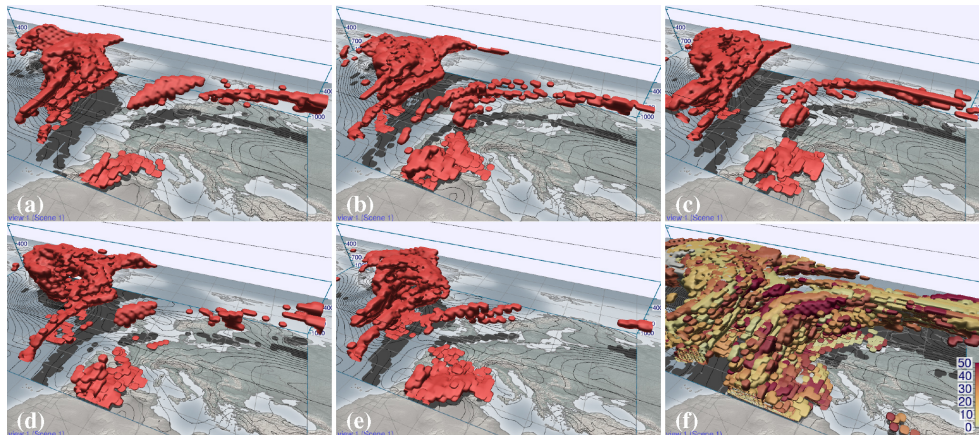


Figure 7. Individual WCB members of the forecast case shown in Fig. 3. Members **(a)** 2, **(b)** 4, **(c)** 34, **(d)** 36 and **(e)** 42. The location and shape of the WCB events vary strongly. **(f)** All 51 members visualized in a single image, distinguished by colour.

3-D visualization of ensemble weather forecasts – Part 2: Warm conveyor belts

M. Rautenhaus et al.

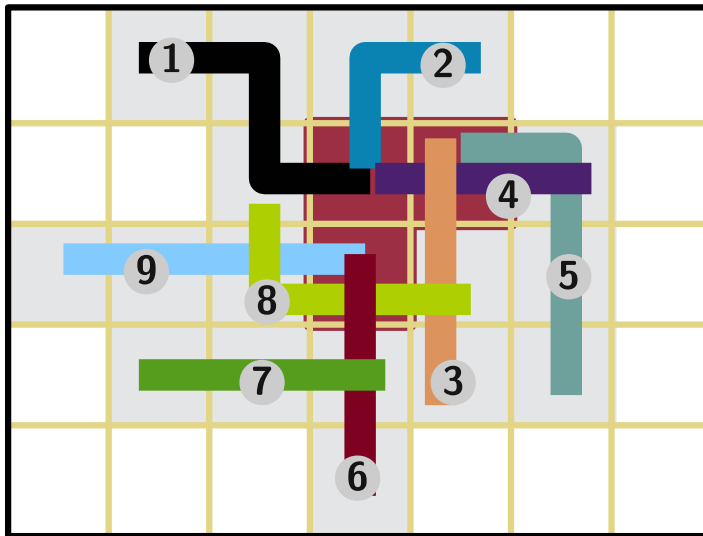


Figure 8. Schematic example of a region of low probability values caused by many members. Of nine members that predict the WCB feature, only a maximum of three overlap in any grid cell. By storing the indices of all members that contribute to a given grid cell, our method is able to determine the members that contribute to a probability region.

[Title Page](#)[Abstract](#)[Introduction](#)[Conclusions](#)[References](#)[Tables](#)[Figures](#)[⏪](#)[⏩](#)[◀](#)[▶](#)[Back](#)[Close](#)[Full Screen / Esc](#)[Printer-friendly Version](#)[Interactive Discussion](#)

3-D visualization of ensemble weather forecasts – Part 2: Warm conveyor belts

M. Rautenhaus et al.

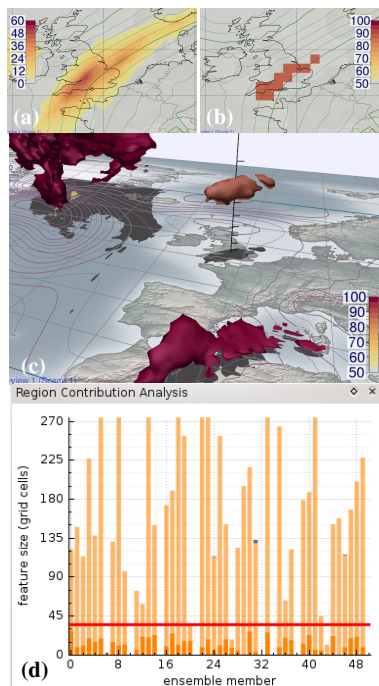


Figure 9. Application of the region contribution algorithm to the WCB forecast from Fig. 3. **(a)** Horizontal section of $p(\text{WCB})$ at 415 hPa over Southern England (colour scale from 0 to 100%). **(b)** The grid boxes exceeding the isosurface threshold of 30 %, as identified by the region growing algorithm (colour scale from 50 to 100 %). **(c)** The 30 % isosurfaces of Fig. 3c coloured by the percentage of contributing members. **(d)** Size (in grid cells) of the WCB features in the contributing members. The red line marks the size of the 30 % isosurface.

3-D visualization of ensemble weather forecasts – Part 2: Warm conveyor belts

M. Rautenhaus et al.

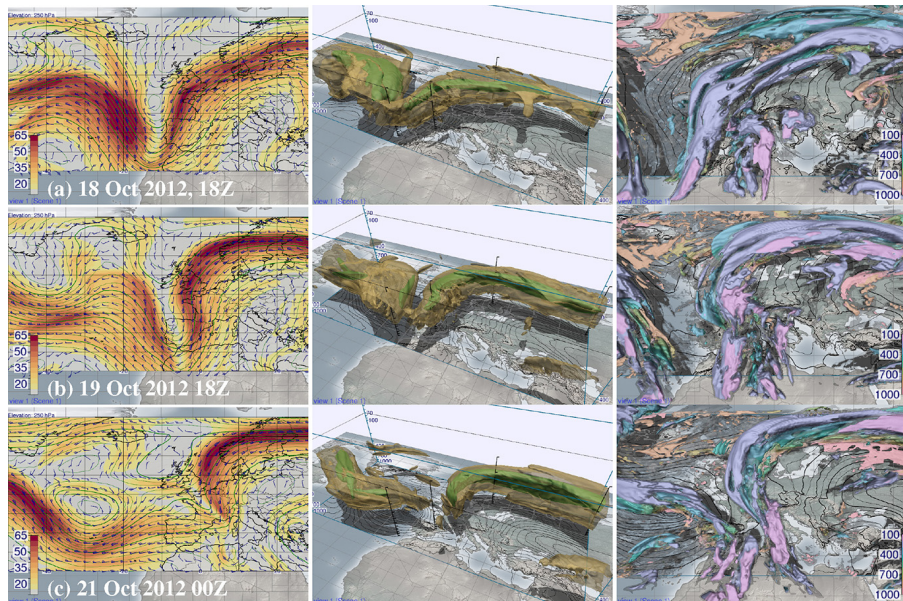


Figure 10. Time sequence of (left) horizontal section with contour lines of geopotential height and filled contours of wind speed (ms^{-1}) at 250 hPa, (middle) jet stream (opaque isosurface 50 ms^{-1} and transparent isosurface 30 ms^{-1}) and (right) clouds (opaque isosurface cloud cover fraction of 0.7 and transparent isosurface cloud cover fraction of 0.2). Colour coding in the right panel denotes cloud elevation in hPa. Deterministic forecast from Monday, 15 October 2012, 00:00 UTC, valid on **(a)** Thursday, 18 October 2012, 18:00 UTC, **(b)** Friday, 19 October 2012, 18:00 UTC, and **(c)** Sunday, 21 October 2012, 00:00 UTC.

Title Page

Abstract

Introduction

Conclusions

References

Tables

Figures

⏪

⏩

◀

▶

Back

Close

Full Screen / Esc

Printer-friendly Version

Interactive Discussion



3-D visualization of ensemble weather forecasts – Part 2: Warm conveyor belts

M. Rautenhaus et al.

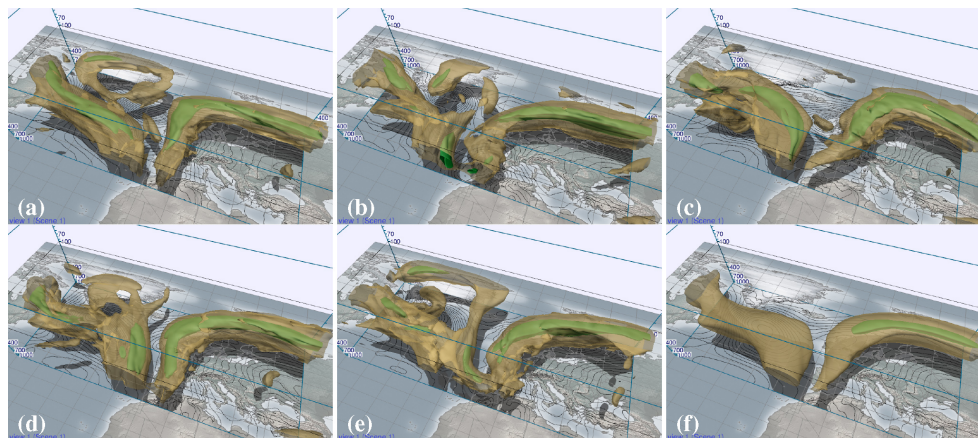
[Title Page](#)[Abstract](#)[Introduction](#)[Conclusions](#)[References](#)[Tables](#)[Figures](#)[Back](#)[Close](#)[Full Screen / Esc](#)[Printer-friendly Version](#)[Interactive Discussion](#)

Figure 11. Navigation through the ensemble. Members **(a)** 27, **(b)** 33, **(c)** 37, **(d)** 43, **(e)** 45 and **(f)** the ensemble mean of horizontal wind speed (forecast from 00:00 UTC on 15 October valid at 18:00 UTC on 19 October 2012). Shown are the 50 ms^{-1} (green opaque) and 30 ms^{-1} (yellow transparent) isosurfaces.

3-D visualization of ensemble weather forecasts – Part 2: Warm conveyor belts

M. Rautenhaus et al.

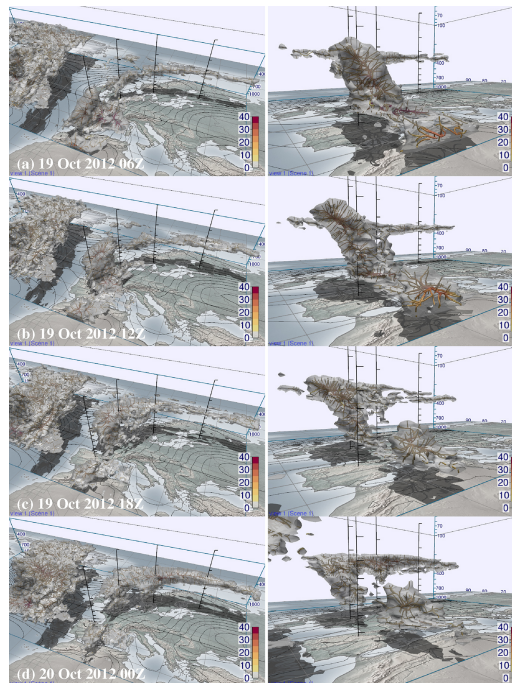


Figure 12. Subsequent time steps of $p(\text{WCB})$ (computed with DF-T setup (S3.)), rendered from different viewpoints. Forecast from 00:00 UTC on 15 October 2012, valid at **(a)** 06:00 UTC, **(b)** 12:00 UTC, **(c)** 18:00 UTC on 19 October and at **(d)** 00:00 UTC on 20 October 2012. Trajectory filtering is set to 500 hPa in 48 h. White isosurface shows a probability of 10%. Normal curves are coloured by probability (%).

[Title Page](#)
[Abstract](#)
[Introduction](#)
[Conclusions](#)
[References](#)
[Tables](#)
[Figures](#)
[⏪](#)
[⏩](#)
[◀](#)
[▶](#)
[Back](#)
[Close](#)
[Full Screen / Esc](#)
[Printer-friendly Version](#)
[Interactive Discussion](#)


GMDD

8, 2161–2212, 2015

3-D visualization of ensemble weather forecasts – Part 2: Warm conveyor belts

M. Rautenhaus et al.

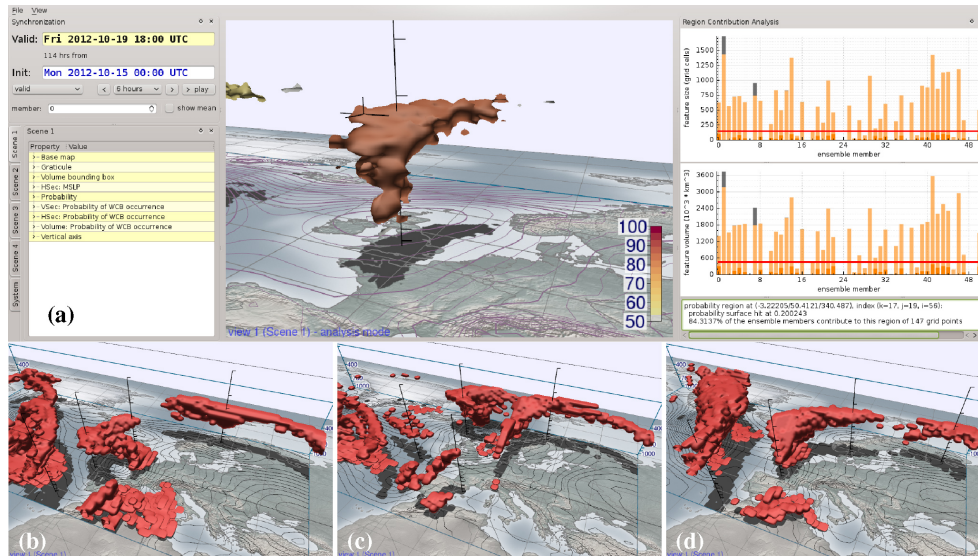


Figure 13. Region contribution analysis applied to the forecast case. **(a)** Screenshot of the Met.3D configuration. The 20% isosurface of $p(\text{WCB})$ is coloured by the percentage of contributing members. The contribution distribution of the feature over Southern England is shown in the histograms on the right side of the window (feature size in (top) grid cells and (bottom) 10^3 km^3). **(b–d)** WCB airmasses for 18:00 UTC on 19 October 2012, as predicted by ensemble members **(b)** 2, **(c)** 9 and **(d)** 19.

Title Page	
Abstract	Introduction
Conclusions	References
Tables	Figures
◀	▶
◀	▶
Back	Close
Full Screen / Esc	
Printer-friendly Version	
Interactive Discussion	



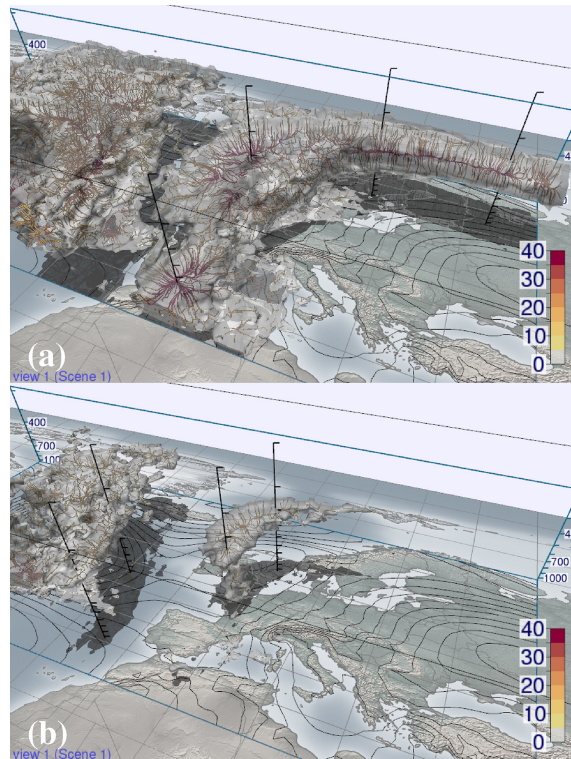


Figure 14. Adjusting the filter criterion for the probability of WCB occurrence. Forecast from 00:00 UTC on 15 October 2012, valid at 18:00 UTC on 19 October 2012. Filter criterion of **(a)** 400 hPa and **(b)** 550 hPa in 48 h. Compare to Fig. 12, in which a criterion of 500 hPa in 48 h is used. Normal curves are coloured by probability (%).

3-D visualization of ensemble weather forecasts – Part 2: Warm conveyor belts

M. Rautenhaus et al.

Title Page

Abstract

Introduction

Conclusions

References

Tables

Figures

⏪

⏩

◀

▶

Back

Close

Full Screen / Esc

Printer-friendly Version

Interactive Discussion



3-D visualization of ensemble weather forecasts – Part 2: Warm conveyor belts

M. Rautenhaus et al.

Title Page

Abstract

Introduction

Conclusions

References

Tables

Figures

◀

▶

◀

▶

Back

Close

Full Screen / Esc

Printer-friendly Version

Interactive Discussion

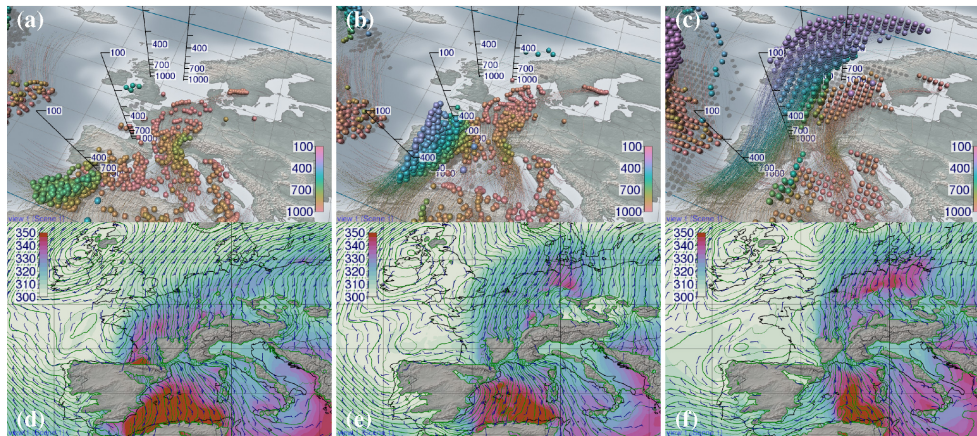


Figure 15. (a–c) Particle positions of the (backward) WCB trajectories of the ensemble control forecast, started on Friday, 19 October 2012, 18:00 UTC and computed on the forecast initialised on Monday, 15 October 2012, 00:00 UTC. Colour codes pressure elevation in hPa. (d–f) Horizontal sections of geopotential height (contour lines), wind barbs and equivalent potential temperature (colour coded in K) of the deterministic forecast from Monday, 15 October 2012, 00:00 UTC at 950 hPa. Forecasts are valid on Thursday, 18 October 2012, 18:00 UTC (a, d) and Friday, 19 October 2012, 06:00 UTC (b, e) and 18:00 UTC (c, f).

3-D visualization of ensemble weather forecasts – Part 2: Warm conveyor belts

M. Rautenhaus et al.

Title Page

Abstract

Introduction

Conclusions

References

Tables

Figures



Back

Close

Full Screen / Esc

Printer-friendly Version

Interactive Discussion

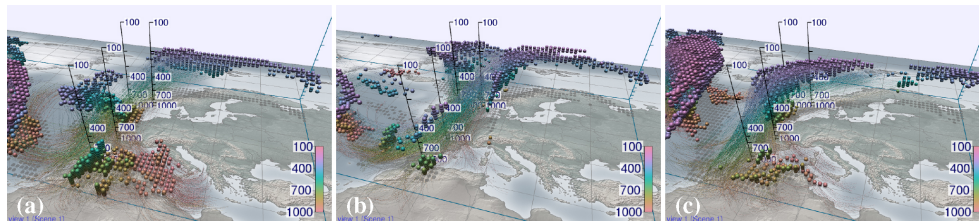


Figure 16. The same as Fig. 15c, but for the ensemble members **(a)** 2, **(b)** 9 and **(c)** 19. Also compare to Fig. 13b–d.

3-D visualization of ensemble weather forecasts – Part 2: Warm conveyor belts

M. Rautenhaus et al.

Title Page

Abstract

Introduction

Conclusions

References

Tables

Figures

◀

▶

◀

▶

Back

Close

Full Screen / Esc

Printer-friendly Version

Interactive Discussion

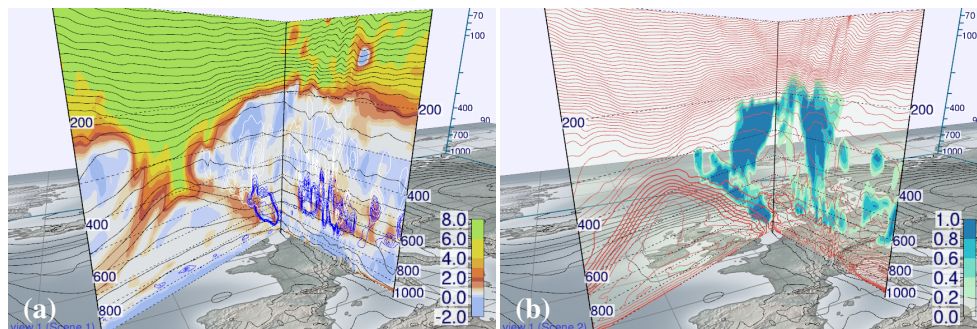


Figure 17. (a) Vertical section of potential vorticity (colour coding in PVU; red colours in the left plot mark the 2-PVU surface and thus the dynamic tropopause), potential temperature (grey contour lines), liquid and ice water content (blue and white contour lines). (b) Vertical section of cloud cover fraction (colour coding) and equivalent potential temperature (red contour lines). Deterministic forecast from 00:00 UTC on Monday, 15 October 2012, valid at 18:00 UTC on Friday, 19 October 2012.

3-D visualization of ensemble weather forecasts – Part 2: Warm conveyor belts

M. Rautenhaus et al.

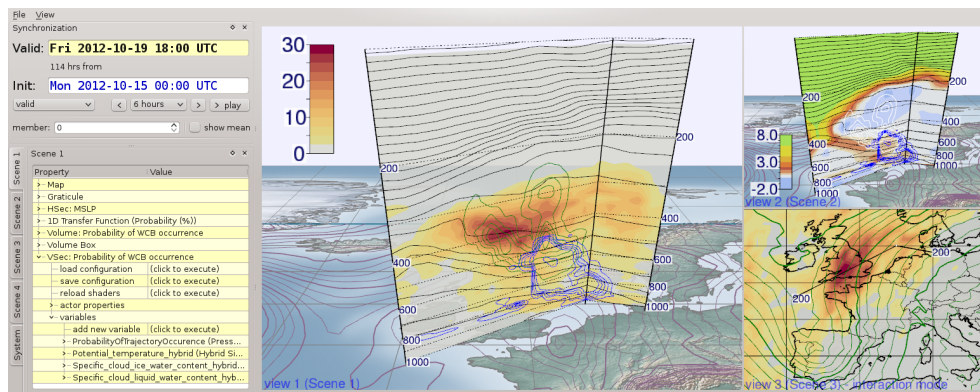


Figure 18. Planning potential flight legs with Met.3D. Large vertical section shows $p(\text{WCB})$ (colour scale in %), small vertical section potential vorticity (colour scale PVU). The horizontal section is located at 390 hPa and also shows $p(\text{WCB})$. The maximum $p(\text{WCB})$ along the proposed leg can be found over southern England at around 400 hPa. The linked views show how a flight at that altitude, going westward, would penetrate the tropopause shortly after sampling the WCB.

Title Page

Abstract

Introduction

Conclusions

References

Tables

Figures

◀

▶

◀

▶

Back

Close

Full Screen / Esc

Printer-friendly Version

Interactive Discussion



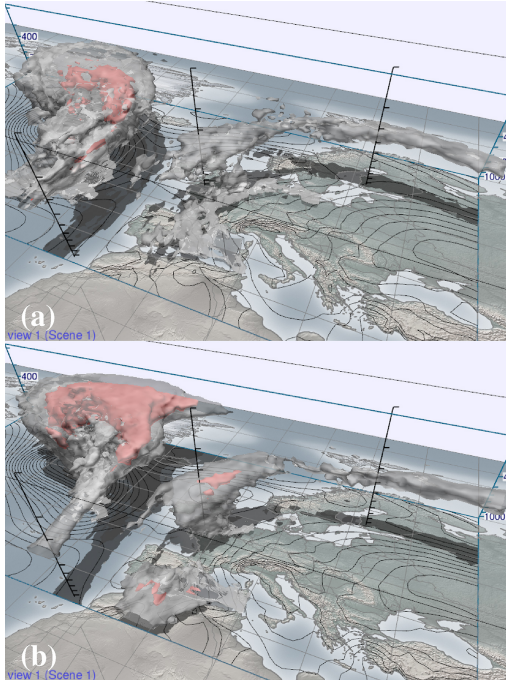


Figure 19. Convergence of the probability of WCB occurrence with decreasing forecast lead time. Forecasts from **(a)** 12:00 UTC on 15 October 2012 and **(b)** 12:00 UTC on 16 October, valid at 18:00 UTC on 19 October 2012. Filter criterion is 500 hPa in 48 h. Isosurfaces show 30 % (red opaque isosurface) and 10 % (white transparent isosurface). The forecast from 00:00 UTC on 17 October 2012 is shown in Fig. 3c.

3-D visualization of ensemble weather forecasts – Part 2: Warm conveyor belts

M. Rautenhaus et al.

[Title Page](#)

[Abstract](#)

[Introduction](#)

[Conclusions](#)

[References](#)

[Tables](#)

[Figures](#)

[◀](#)

[▶](#)

[◀](#)

[▶](#)

[Back](#)

[Close](#)

[Full Screen / Esc](#)

[Printer-friendly Version](#)

[Interactive Discussion](#)

